



Trans. Nonferrous Met. Soc. China 22(2012) 2402-2408

Transactions of Nonferrous Metals Society of China

www.tnmsc.cn

# Microstructural evolution of zirconium alloy under dynamic compression at strain rate of 1000 s<sup>-1</sup>

ZOU Dong-li, LUAN Bai-feng, LIU Qing

College of Materials Science and Engineering, Chongqing University, Chongqing 400044, China Received 9 July 2012; accepted 10 August 2012

Abstract: Microstructural evolution of the zirconium alloy deformed at a strain rate of about  $1000 \text{ s}^{-1}$  was investigated. Four different strain levels of the zirconium alloy subjected to dynamic compression were designed by several-times impacting at almost the same strain rate. The results show that abundant low angle boundaries at different strain levels were observed in the deformed microstructures, and the quantity and density of low angle boundary increase dramatically with the strain increasing. Besides low angle boundaries and high angle boundaries observed in grain boundary maps, the twin boundaries including the tensile twins  $\{10\overline{1}2\}$ ,  $\{11\overline{2}1\}$  and compressive twins  $\{11\overline{2}2\}$  were distinguished at different strain levels, and most twin boundaries were indexed as  $\{10\overline{1}2\}$  twins. With the stain increasing, the twin boundary density in the deformed microstructures increases indistinctively. Based on the characterization of the deformed microstructures at the different strain levels, the deformation and evolution processes of the zirconium alloy subjected to dynamic loading were proposed. Microhardness measurements show that the microhardness in the impacted specimens increases gradually with the strain increasing, which should be associated with the strain hardening caused by the tangled dislocation.

Key words: zirconium alloy; dynamic compression; plastic deformation

#### 1 Introduction

Zirconium alloy as the fuel cladding material has been widely used in the nuclear power reactors due to its high melting point, low neutron absorption cross section, good corrosion resistance and excellent mechanical properties. Before application, the blasting tests, as an important service property, for the zirconium alloy tubes should be conducted to ensure the security of the nuclear power reactors. Thus, the dynamic deformation behaviors of the zirconium alloy should be paid attention to.

The main difference between the dynamic and quasi-static deformation is the strain rate, and rarely observed deformed microstructures under quasi-static deformation can be induced by dynamic deformation. Furthermore, the deformed microstructures under both dynamic and quasi-static loading conditions are closely related with the deformation and fracture processes, leading to the wide interests in investigating the

deformed microstructures for enunciating deformation process of the materials. As reported, various deformed microstructures of the materials subjected to dynamic loadings have been observed, such as dislocation structures [1,2], deformation twins [3,4], adiabatic shear bands [5,6], dynamic recrystallized grains [7,8], and phase transformed microstructures [9]. However, limited results referring in the deformed microstructures of the zirconium alloy subjected to dynamic loading are available [10,11], leading to the deformation process in zirconium alloy subjected to dynamic deformation still unclearly. Therefore, a systematic investigation of the deformed microstructures in zirconium alloy subjected to dynamic loading is necessary for understanding the deformation process.

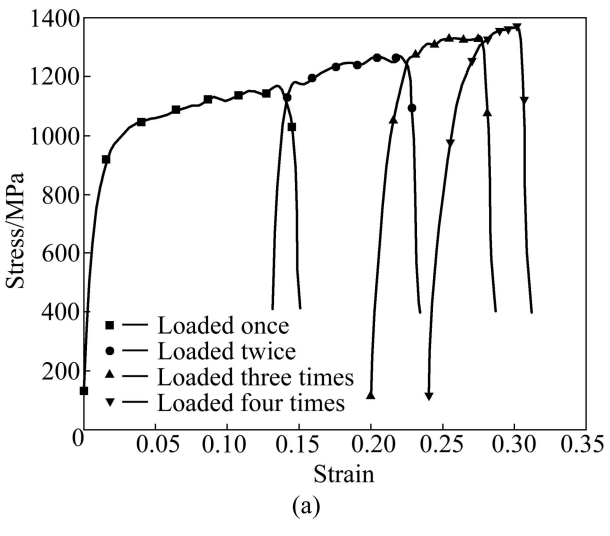
In this work, four different strain levels of the zirconium alloy deformed at a strain rate of about 1000 s<sup>-1</sup> are designed, and the corresponding microstructures are characterized for understanding its deformation behaviors under dynamic loading.

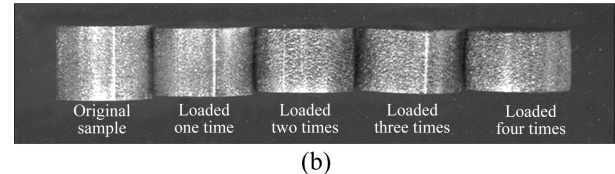
### 2 Experimental

The annealed zirconium plate with thickness of 4.6 mm was selected as the experimental material, and its chemical compositions in mass fraction were: 1.20%-1.70% Sn. 0.18%-0.24% Fe. 0.07%-0.13% Cr. The cylindrical specimens with c axis parallel to the normal direction (ND) were cut from the plate, and the diameter and height of the specimens were 6 mm and 4.6 mm, respectively. Dynamic impact experiments were conducted on a split Hopkinson pressure bar (SHPB), and the strain rate for every impacting was kept constant, about 1000 s<sup>-1</sup>. The metallographic specimens were cut along the rolling direction (RD), then polished and etched in a solution of 45 mL H<sub>2</sub>O + 45 mL HNO<sub>3</sub> + 10 mL HF, and a final anodization step was performed on the specimens [10]. The metallographic specimens were observed by an optical microscope (OM) with a polarized light mode (ZEISS Axiovert 40). Electron backscatter diffraction (EBSD) specimens were prepared by electropolishing in a solution of 70 mL CH<sub>3</sub>OH + 20 mL  $C_6H_{14}O_2 + 10$  mL  $HClO_4$ , and the polishing voltage and temperature were kept at 20 V and -30 °C, respectively. EBSD tests were performed on a FEG-SEM (FEI Nova 400) with a HKL-EBSD system (Oxford HKL Channel-5) operated at 20 kV. The transmission electron microscopy (TEM) specimens were prepared by ion-milling, and the observations were carried out on a ZEISS microscope operated at 200 kV. Following optical metallographic observation, Vickers microhardness was measured by a MH-5L microhardness tester. A load of 9.8 N and a dwell time of 15 s were employed during microhardness measurements.

#### 3 Results and discussion

Figure 1 shows the stress—strain curve and macroscopic images of the impacted specimens at different strain levels. The strain of about 0.14 is obtained by impacting once, while the strain levels of about 0.22 and 0.27 are obtained by impacting twice and three times, respectively. After impacting four times, the total strain level of about 0.31 is acquired. During dynamic compression, the strain increments decrease gradually after every impacting, from 0.14 at first to 0.04 at the fourth times, which should be associated with the strain hardening. High strength caused by strain hardening leads to the strain level decreasing at almost the same impact velocity. Under dynamic compression, the stress—strain curve presents the distinct strain hardening, and almost no thermal softening behavior can





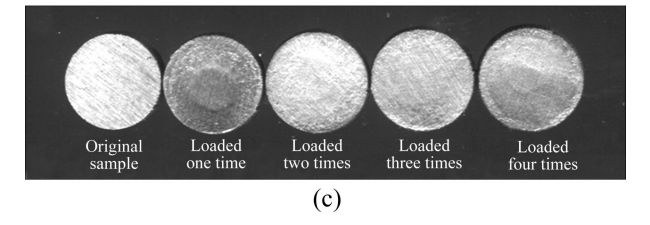
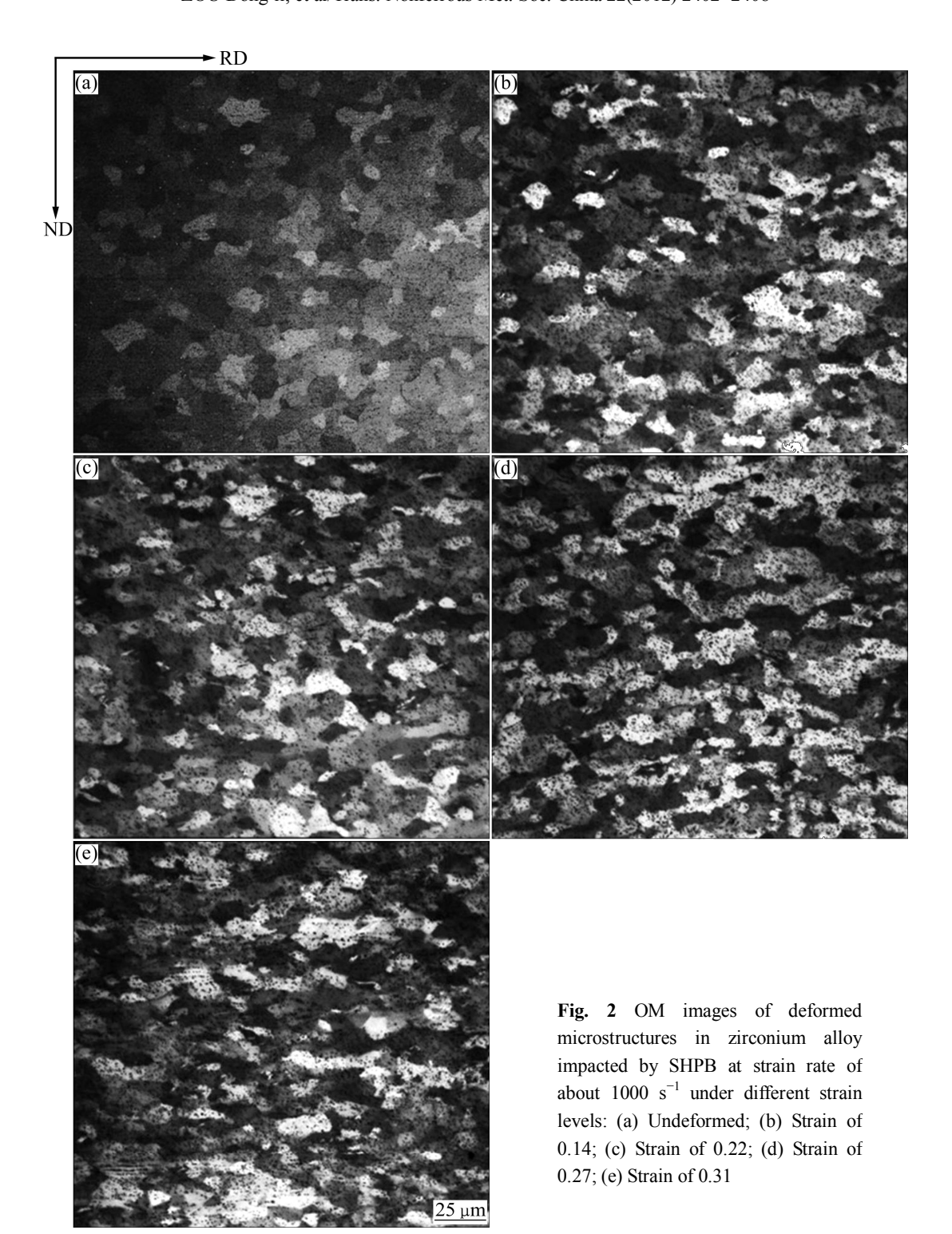


**Fig. 1** Stress—strain curve (a) and macroscopic, front view (b) and top view (c) of specimens impacted by SHPB at strain rate of about  $1000 \text{ s}^{-1}$ 

be observed, as shown in Fig. 1(a). The macroscopic views of the specimens impacted by SHPB are shown in Figs. 1(b) and (c). After every impacting, the specimen heights reduce, and the corresponding specimen diameters increase, indicating that the strain levels of materials increase gradually.

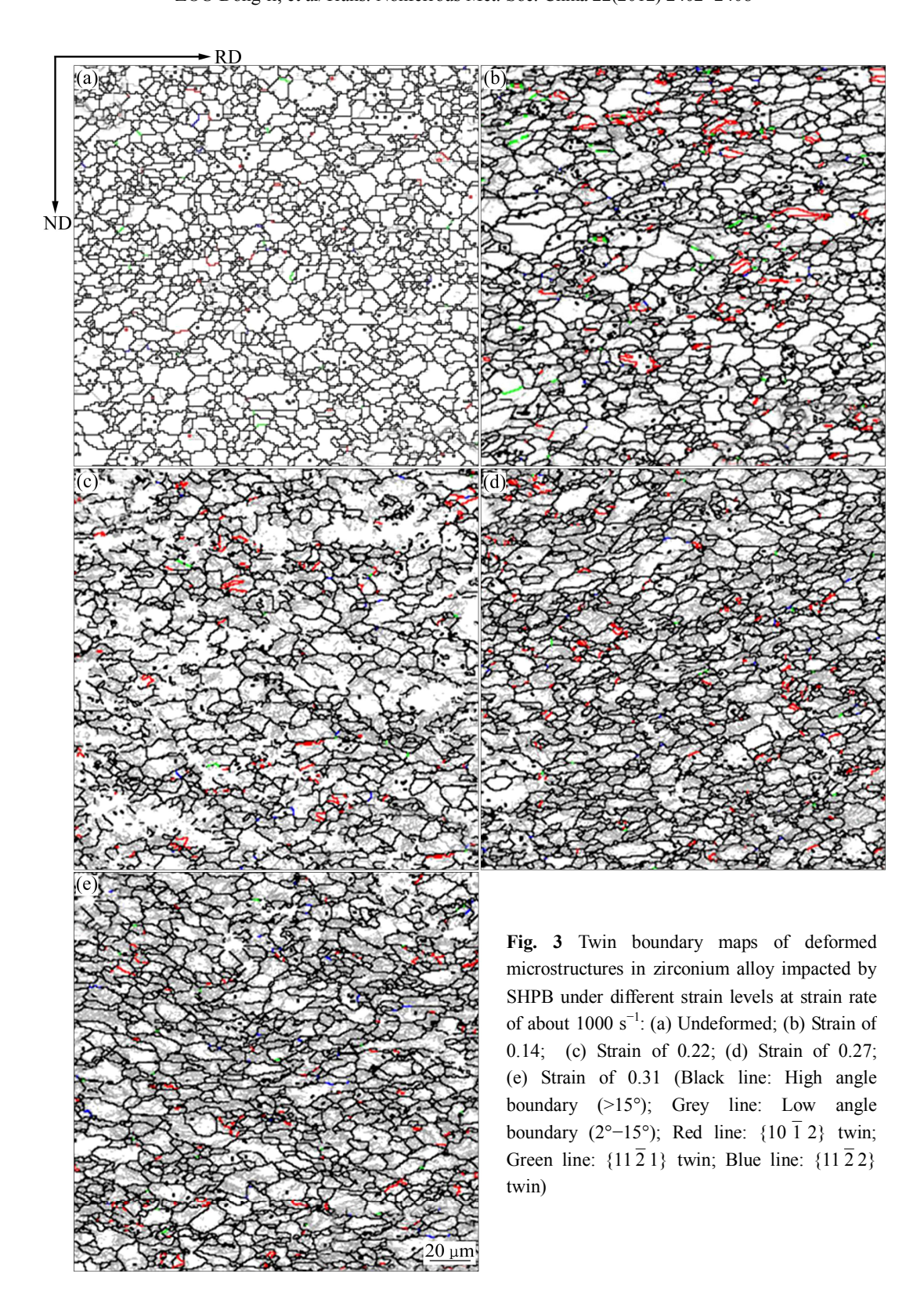
OM images of the deformed microstructures in zirconium alloy subjected to different strain levels are shown in Fig. 2. The undeformed specimens composed of the equiaxed grains with diameter ranging from 10 to 20 µm can be observed in Fig. 2(a). With the strain increasing from 0.14 to 0.31, the grains in zirconium alloy are elongated gradually, and the elongated direction of the severely deformed grains is consistent with the RD. At a large strain, the severe plastic deformation leads to the grain boundary difficult to distinguish, indicating that high density dislocations are piled up at the grain boundary. Under the different strain levels, a few twin laths can be observed in the deformed microstructures, and no adiabatic shear band or strain localization phenomenon is detected, indicating that the twinning as



well as shear band is not the main plastic deformation mechanism of the zirconium alloy subjected to dynamic loading at the strain up to 0.31 and a strain rate of about  $1000~\text{s}^{-1}$ .

Figure 3 shows the grain boundary maps of the deformed microstructures in zirconium alloy subjected to different strain levels, and the corresponding statistically relative frequencies of the grain boundary including low angle boundary (LAB) and high angle boundary (HAB)

are shown in Fig. 4. By comparison, the statistical grain boundary of the original sample is added in Fig. 4. In the original sample, the statistically relative frequency of LAB to HAB is about 28.1%. With the strain increasing to 0.14, the relative frequency of LAB to HAB increases dramatically, from 28.1% to 69.8%, further indicating that lots of dislocations are triggered. With the strain increasing from 0.14 to 0.31, the relative frequency of LAB to HAB increases gradually, and the maximum



relative frequency of LAB to HAB of about 79.4% is obtained at a strain of 0.31. Apart from LAB and HAB, the twin boundaries are observed and distinguished in grain boundary maps at different strain levels. According to previous reports [12,13], three twin modes including  $\{10\overline{1}2\}$ ,  $\{11\overline{2}1\}$  and  $\{11\overline{2}2\}$  could be activated at

room temperature under both tension and compression loading, and the  $\{10\,\overline{1}\,1\}$  twin could be only triggered at the elevated temperature. In our experimental results, the severely dynamic deformation leads to three twin modes including  $\{10\,\overline{1}\,2\}$ ,  $\{11\,\overline{2}\,1\}$  and  $\{11\,\overline{2}\,2\}$  appearing in the deformed microstructures at different strain levels,

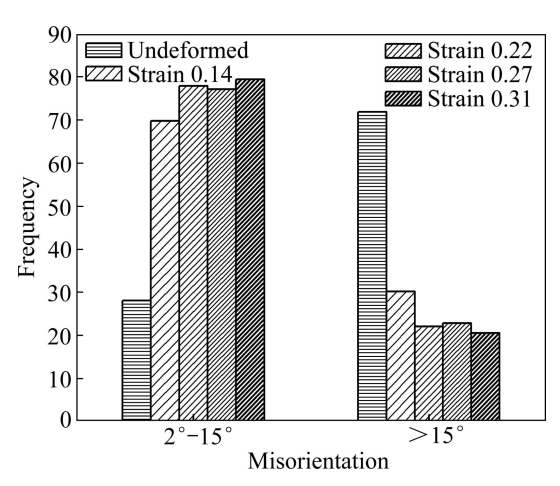


**Fig. 4** Statistical misorientation in specimens deformed at different strain levels impacted by SHPB at strain rate of about  $1000 \, \text{s}^{-1}$ 

and the tensile twins  $\{10\overline{1}2\}$  play a dominant role, which should be associated with the shear displacement and critical shear stress. As reported, the calculated shear displacements for the deformation twins  $\{10\ \overline{1}\ 2\}$ ,  $\{11\overline{2}2\}$  and  $\{11\overline{2}1\}$  in zirconium alloy were about 0.17, 0.23 and 0.63, respectively [13,14]. Small shear displacement assisted with low critical shear stress leads to the  $\{10\overline{1}2\}$  tensile twins activated in the deformed microstructures in zirconium alloy easily. With the strain increasing from 0.14 to 0.31, the density of the twin boundaries increases indistinctively, indicating that the twinning plays an assistant role on the plastic deformation of the zirconium alloy subjected to dynamic loading at a stain rate of about 1000 s<sup>-1</sup>. Compared with the quasi-static deformation, dynamic deformation leads to the deformation twins formed in zirconium alloy, and almost no deformation twins in zirconium alloy can be activated by quasi-static deformation. Thus, the main microstructural difference between the dynamic and quasi-static deformation is the deformation twins. Under high strain-rate deformation, dislocation slipping cannot accommodate the local strain due to the rapidly plastic deformation, leading to the local stress concentration to trigger the deformation twins. In addition, abundant adiabatic shear bands have been observed in various materials subjected to the dynamic deformation, and the adiabatic shear bands were considered an important plastic deformation mechanism of the materials subjected to the dynamic loadings. However, the adiabatic shear bands, especially the transformed bands, are difficult to form in the materials under the quasi-static deformation. Thus, the adiabatic shear bands are also regarded as the microstructural difference for the materials deformed under the dynamic and quasi-static loadings. Thermal accumulation in a local area because

of insufficient heat diffusion is considered the formation reason of the adiabatic shear bands in many materials. In our experimental results, no adiabatic shear band is detected due to the low strain rate and strain levels of the materials suffered. Therefore, the microstructural difference in zirconium alloy in our experiments between the dynamic and quasi-static deformation is the deformation twins.

TEM images of the deformed microstructures in zirconium alloy subjected to different strain levels are shown in Fig. 5. High density dislocation can be observed at different strain levels, and the dislocation density increases with the strain increasing from 0.14 to 0.31. At a strain of about 0.31, lots of subgrains in the deformed microstructures can be observed, which should be associated with the interaction of high density dislocation. However, twin laths distinguished by EBSD are not found by TEM observation because of the limitation of the number. As reported, the c/a axial ratio had a dominant influence on the slipping systems to be activated [12]. As for the zirconium alloy, the c/a axial ratio is smaller than the ideal sphere packing (c/a=1.633), and the prismatic slipping with  $<11\overline{2}$  0> direction is considered the main dislocation slipping mode of the zirconium alloy at room temperature due to the low critical resolved shear stress [13,15]. Besides the prismatic slipping, in the stress concentration or the severe deformation zones, the basal slipping with  $<11\overline{2}$  0> direction and the pyramidal slipping with  $<11\overline{2}$  3> direction in zirconium alloy were observed and confirmed [16,17], leading to the zirconium alloy exhibiting a good ductility. Thus, the prismatic slipping, the basal slipping and the pyramidal slipping are considered the main dislocation slipping modes of the zirconium alloy subjected to dynamic loading, and  $\{10\ \overline{1}\ 0\}$  prismatic slipping and  $\{10\ \overline{1}\ 1\}$  pyramidal slipping play a dominant role [13,18].

Based on the characterization of the deformed microstructures at different strain levels, the deformation and evolution processes of the deformed microstructures in zirconium alloy subjected to dynamic loading can be depicted. At the initial stage, the {10 1 0} prismatic slipping is proposed as the primary plastic deformation mechanism of the zirconium alloy [19]. With the strain increasing, the pyramidal slipping and  $\{10\overline{1}2\}$  twins can be activated to accommodate the plastic deformation of the zirconium alloy because of high local shear stress. With the strain proceeding, high density prismatic and pyramidal dislocations in the preferential oriented grains can be triggered by high stress and strain levels, but the deformation twins are difficult to be activated ulteriorly because of small grain size in zirconium alloy, leading to the twin density at different strain levels unchanged

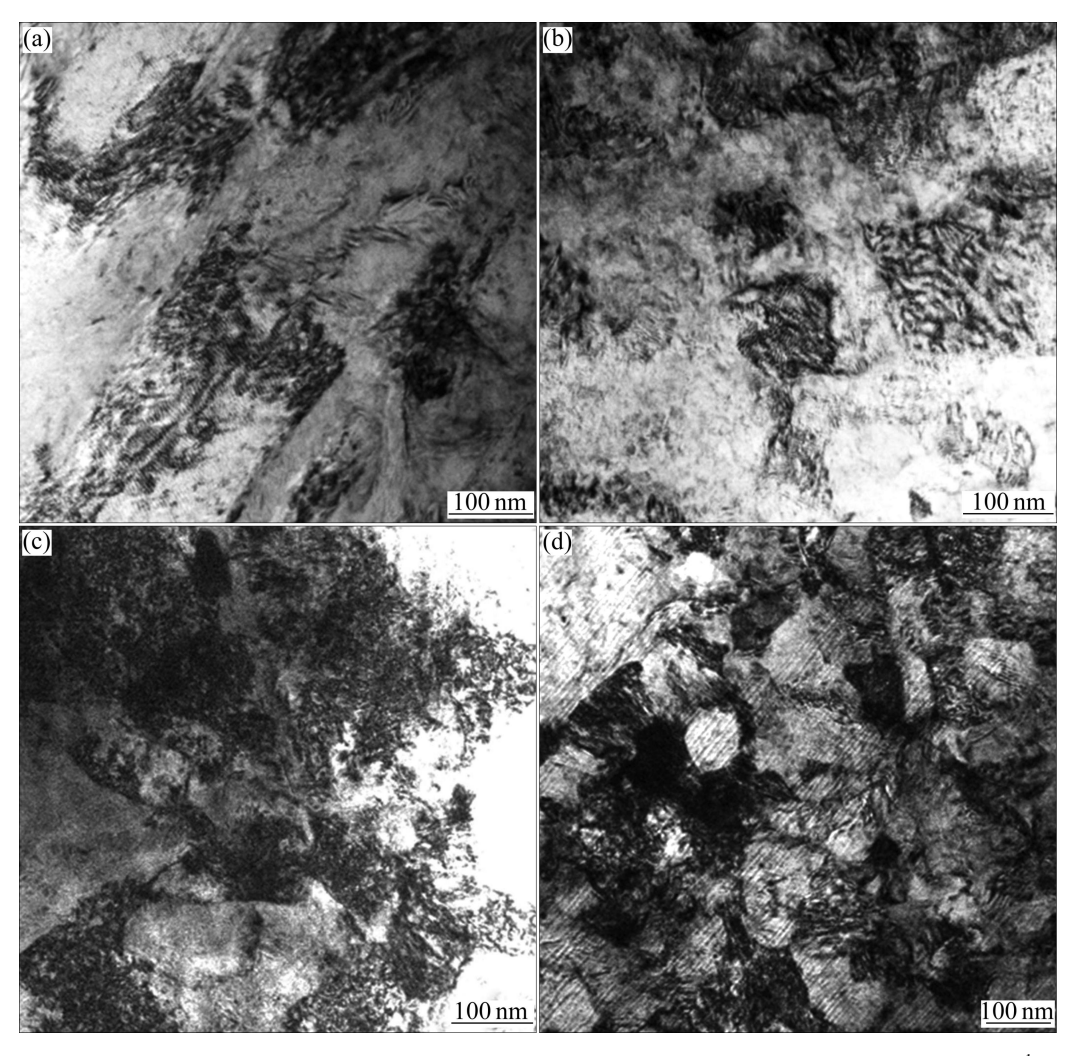


**Fig. 5** TEM images of deformed microstructures in zirconium alloy impacted by SHPB at strain rate of about 1000 s<sup>-1</sup> under different strain levels: (a) 0.14; (b) 0.22; (c) 0.27; (d) 0.31

distinctively. With the strain proceeding, high density dislocation can be slipped and interacted with each other, leading to the formation of the subgrains. When the strain increases to the critical point, the deformed microstructures can be saturated by high density dislocation, then the dislocation slipping cannot accommodate the plastic deformation further, leading to strain localization to form the shear bands or cracks, finally breaking into fragments.

Vickers microhardness values of the specimens deformed at different strain levels are shown in Fig. 6. By comparison, the microhardness of the original sample was measured. It can be noted that the microhardness increases with the strain increasing, and the maximum microhardness of about HV206 is obtained at a strain of about 0.31, which is about 1.2 times higher than that of the original sample. High microhardness in the deformed specimens should be associated with the strain hardening caused by tangled and piled dislocations.

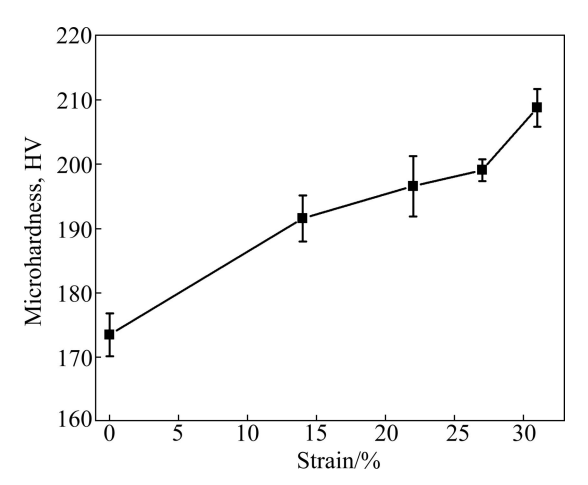


**Fig. 6** Vickers microhardness in specimens impacted by SHPB at different strain levels and at strain rate of about  $1000 \text{ s}^{-1}$ 

#### **4 Conclusions**

1) Different strain levels of the zirconium alloy subjected to the dynamic loading are designed by means

of impacting several times at almost the same strain rate, and four different strain levels about 0.14, 0.22, 0.27 and 0.31 are obtained.

- 2) The  $\{10\ \overline{1}\ 0\}$  prismatic slipping,  $\{10\ \overline{1}\ 1\}$  pyramidal slipping and  $\{10\ \overline{1}\ 2\}$  tensile twin are considered the main deformation mechanism for zirconium alloy subjected to different strain levels.
- 3) Microstructural evolution of the zirconium alloy subjected to dynamic deformation was proposed by the characterization of the deformed microstructures at different strain levels.
- 4) Strain hardening leads to the microhardness in the deformed specimens higher than that of the original sample.

#### References

- [1] MURR L E, FERREYRA T E, PAPPU S, GARCIA E P, SANCHEZ J C, HUANG W, RIVAS J M, KENNEDY C, AYALA A, NIOU C S. Novel deformation process and microstructures involving ballistic penetrator formation and hypervelocity impact and penetration phenomena [J]. Materials Characterization, 1996, 37: 245–276.
- [2] ZHOU J S, YANG D Z. The dislocation configuration and its formation mechanism under dynamic loading condition [J]. Material Science and Technology, 1997, 5: 13–17.
- [3] MEYERS M A, XU Y B, XUE Q, PEREZ-PRADO M T, MCNELLEY T R. Microstructural evolution in adiabatic shear localization in stainless steel [J]. Acta Materialia, 2003, 51: 1307– 1325.
- [4] HUANG Wen, WANG Yang, LI Zi-ran, XIA Yuan-ming. Influences of temperature and strain rate on deformation twinning of polycrystalline titanium [J]. The Chinese Journal of Nonferrous Metals, 2008, 18(8): 1440–1445. (in Chinese)
- [5] YANG Yang, CHENG Xin-lin. Current status and trends in researches on adiabatic shearing [J]. The Chinese Journal of Nonferrous Metals, 2002, 12(3): 401–408. (in Chinese)

- [6] CHICHILI D R, RAMESH K T, HEMKER K J. Adiabatic shear localization in α-titanium: Experiments, modeling and microstructural evolution [J]. Journal of the Mechanics and Physics of Solids, 2004, 52: 1889–1909.
- [7] MURR L E, ESQUIVEL E V. Observation of common microstructural issues associated with dynamic deformation phenomena: Twins, microbands, grain size effects, shear bands, and dynamic recrystallization [J]. Journal of Materials Science, 2004, 39: 1153-1168
- [8] LIN Jun-pin, CHENG Jing-wei. Dynamic recrystallization during hot torsion of Al-2Mg alloy [J]. The Chinese Journal of Nonferrous Metals, 1999, 9(3): 510–514. (in Chinese)
- [9] HSIUNG L M, LASSILA D H. Shock-induced omega phase in tantalum [J]. Scripta Materialia, 1998, 38: 1371–1376.
- [10] KAD B K, GEBERT J M, PEREZ-PRADO M T, KASSNER M E, MEYERS M A. Ultrafine-grain-sized zirconium by dynamic deformation [J]. Acta Materialia, 2006, 54: 4111–4127.
- [11] XIAO D W, LI Y L, HU S S, CAI L C. High strain rate deformation behavior of zirconium at elevated temperatures [J]. Journal of Materials Science and Technology, 2010, 26: 878–882.
- [12] MURTY K L, CHARIT I. Texture development and anisotropic deformation of zircaloys [J]. Progress in Nuclear Energy, 2006, 48: 325–359.
- [13] TENCHHOFF E. Review of deformation mechanisms. texture, and mechanical anisotropy in zirconium and zirconium base alloys [J]. Journal of ASTM International, 2005, 2: 1–26.
- [14] YOO M H. Slip, twinning, and fracture in hexagonal close-packed metals [J]. Metallurgical Transactions A, 1981, 12: 409–418.
- [15] RAPPERPORT E J. Room temperature deformation processes in zirconium [J]. Acta Metallurgica, 1959, 7: 254–260.
- [16] DICKSON J I, CRAIG G B. Room temperature basal slip in zirconium [J]. Journal of Nuclear Materials, 1971, 40: 346–348.
- [17] AKHTAR A. Basal slip in zirconium [J]. Acta Metallurgica, 1973, 21: 1–11.
- [18] NUMAKURA H, MINONISHI Y, KOIWA M. < 1 1 23>{10 1 1} slip in zirconium [J]. Philosophical Magazine A, 1991, 63: 1077–1084.
- [19] YOO M H, AGNEW S R, MORRIS J R, HO K M. Non-basal slip systems in HCP metals and alloys: Source mechanisms [J]. Materials Science and Engineering A, 2001, 319–321: 87–92.

## 锆合金在应变速率 1000 s<sup>-1</sup> 下动态压缩显微组织的演化规律

邹东利,栾佰峰,刘 庆

重庆大学 材料科学与工程学院, 重庆 400044

摘 要:研究锆合金在应变速率 1000 s<sup>-1</sup> 动态压缩条件下的显微组织演化规律。基于相同应变速率下多次撞击的方法实现锆合金动态压缩下 4 个不同的应变水平。在不同的应变水平下,应力一应变曲线具有明显的应变硬化效应,几乎观察不到明显的热软化效应。标定的晶粒边界图像表明,在不同的应变水平下,在变形组织内均可观察到大量的小角晶界,同时,小角晶界的数量和密度随着应变的增加而增多。除了在晶粒边界图像中观察到的小角晶界和大角晶界外,在不同的应变水平下还可观察到孪晶界。孪晶界的类型主要包括{10 12}、{11 21}拉伸孪晶和{11 22}压缩孪晶,且大多数孪晶界为{10 12}拉伸孪晶。随着应变水平的增加,变形组织中孪晶界的密度变化不明显。基于不同应变水平下变形组织的表征,提出了动态载荷下锆合金变形和演化过程。显微硬度测试表明,撞击试样的硬度随着应变的增加而逐渐增大,这主要与位错塞积引起的应变硬化有关。

关键词: 锆合金; 动态压缩; 塑性变形